Appl. Math. Mech. -Engl. Ed., **39**(3), 437–454 (2018)

Applied Mathematics and Mechanics (English Edition)

https://doi.org/10.1007/s10483-018-2305-9

Fallopian tube assessment of the peristaltic-ciliary flow of a linearly viscous fluid in a finite narrow tube*

H. ASHRAF[1,†], A. M. SIDDIQUI[2], M. A. RANA[1]

1. Department of Mathematics and Statistics, Riphah International University, Sector I-14, Islamabad 56180, Pakistan;
2. Department of Mathematics, York Campus, Pennsylvania State University, York, Pennsylvania 17403, U. S. A.

(Received Apr. 13, 2017 / Revised Aug. 10, 2017)

Abstract The present theoretical assessment deals with the peristaltic-ciliary transport of a developing embryo within a fallopian tubal fluid in the human fallopian tube. A mathematical model of peristalsis-cilia induced flow of a linearly viscous fluid within a fallopian tubal fluid in a finite two-dimensional narrow tube is developed. The lubrication approximation theory is used to solve the resulting partial differential equation. The expressions for axial and radial velocities, pressure gradient, stream function, volume flow rate, and time mean volume flow rate are derived. Numerical integration is performed for the appropriate residue time over the wavelength and the pressure difference over the wavelength. Moreover, the plots of axial velocity, the appropriate residue time over wavelength, the vector, the pressure difference over wavelength, and the streamlines are displayed and discussed for emerging parameters and constants. Salient features of the pumping characteristics and the trapping phenomenon are discussed in detail. Furthermore, a comparison between the peristaltic flow and the peristaltic-ciliary flow is made as the special case. Relevance of the current results to the transport of a developing embryo within a fallopian tubal fluid from ampulla to the intramural in the fallopian tube is also explored. It reveals the fact that cilia along with peristalsis helps to complete the required mitotic divisions while transporting the developing embryo within a fallopian tubal fluid in the human fallopian tube.

Key words peristaltic-ciliary flow, linearly viscous fluid, analytic solution, human fallopian tube

Chinese Library Classification O357.1
2010 Mathematics Subject Classification 76D05, 76D08, 92C10, 92C35

1 Introduction

In the human female abdominal cavity, there exist either a pair of long muscular and narrow tubes called "fallopian tube". Each fallopian tube is of 10 cm to 13 cm in length and 0.5 cm to

* Citation: Ashraf, H., Siddiqui, A. M., and Rana, M. A. Fallopian tube assessment of the peristaltic-ciliary flow of a linearly viscous fluid in a finite narrow tube. *Applied Mathematics and Mechanics* (*English Edition*), **39**(3), 437–454 (2018) https://doi.org/10.1007/s10483-018-2305-9

† Corresponding author, E-mail: hameedashraf09@yahoo.com

1.2 cm in diameter. A fallopian tube has cyclic peristaltic contractions, and the inner surface is lined with a layer of mucous membrane. The mucous membrane is crowded with secretory and ciliated cells of different heights. Each cilium is about 10 μm long and 0.25 μm in diameter[1–10]. Secretory cells pour out a small volume of fallopian tubal fluid, which helps to keep sperm, ovum, and embryo alive and nourish the developing embryo as it is transported towards the uterus[11–12]. Ciliated cells have hair like structures whose swaying motions generate metachronal wave[13–15]. The cyclic peristaltic contractions of the fallopian tube surface generate sinusoidal wave[16–25]. The sinusoidal wave and the metachronal wave are in continuum and merge together to generate a travelling wave. The fluid flow induced by such travelling wave terms is a peristaltic-ciliary flow. The peristaltic-cilia flow is considered to be a major source of transportation in the fallopian tube. The peristaltic-cilia flow in the fallopian tube assists the self propulsion of spermatozoa towards ampulla in the preovulatory phase and facilitates the transportation of the ovum from the ovaries at the time of ovulation. If fertilization occurs at ampulla successfully, the peristaltic-cilia flow transports the developing embryo within the fallopian tubal fluid to intramural, the last region of the fallopian tube[6–9]. Accordingly, the cyclic peristaltic contractions and the action of cilia tips together play an important role in transporting the developing embryo from the ampulla to the intramural of the fallopian tube. The developing embryo then enters the non-pregnant uterus where only peristaltic contractions of the uterus are present to provide an assistance for implantation during the early process of human reproduction[8,10].

A fallopian tube is composed of four regions: infundibulum, ampulla, isthmus, and intramural. The infundibulum region which lies near the ovaries is approximately of 1 cm to 2 cm in length. This region includes finger like fimbria, whose movements are muscle controlled and densely ciliated, forming a funnel-shaped depository for the capturing of cumulus-oocyte complex. The ampulla, a highly ciliated central portion of the fallopian tube, averages 6 cm to 8 cm in length, within which the fertilization of ovum by spermatozoa and the initial development of embryo occur. The isthmus, a less densely ciliated region of the fallopian tube, is approximately of 2 cm to 3 cm in length. In this region, the transportation of sperm from uterus to ampulla in the preovulatory phase and embryo from ampulla to uterus after fertilization is regulated. Mitotic divisions in a developing embryo also take place in this region (isthmus region). Intramural (averaged length 1 cm) is the last region of the fallopian tube. It is likewise isthmus, a less densely ciliated region of the fallopian tube. It is located within the myometrium of the uterus and connects isthmus of the fallopian tube with the fundus of the uterus, at which the fallopian tube empties and where developing embryo is to be implanted[1,3,7–8].

The process of human reproduction begins successfully when a spermatozoon and an ovum fuse to become an embryo at the ampulla. Soon after fertilization, the initial development begins in the form of mitotic divisions. The developing embryo is then transported within the fallopian tubal fluid by a travelling wave. The process of first mitotic division begins which includes the male and female chromosomes mingling, the replication and division of chromosomes. The process of first mitotic division still continues, while the developing embryo within the fallopian tubal fluid then enters the isthmus region. In this region, the embryo undergoes several mitotic divisions to become a ball of 32 cells, called the morula. The morula continues dividing as it is transported within the fallopian tubal fluid to the intramural region. Now the developing embryo is a large mass of cells, called the early blastocyst (a fluid filled cavity), which then enters the uterus where only peristaltic contractions of the uterus surface assist the transportation of developing embryo. The late blastocyst with an inner cell mass about 100 μm−150 μm in size, enters the fundus whereby it attaches to the lining of the fundus, a process called implantation, and is completed to develop into pregnancy. About 42 mitotic cell divisions take place to produce a newborn baby. These cells form and function: some nerve cells, some liver cells, some becoming muscle cells, and so on[2,5–6,8–9].

Eytan and Elad[26] and Eytan et al.[27] incorporated the applications of the peristaltic flow of

incompressible linearly viscous fluid in a finite channel to the transport of an embryo within the intrauterine/fallopian tubal fluid. Later, Yaniv et al.[28] simulated the flow of an incompressible linearly viscous fluid in a closed uterine cavity. However, they neglected the role of the cilia tips despite the fact that Blake et al.[29] showed that the cilia alone was sufficient to drive a fluid flow in the fallopian tube. Wakeley[10] developed his own model in which both the cyclic peristaltic contractions of the channel wall and the swaying motions of the cilia tips which lined the interior surfaces of the channel walls generated the fluid flow pattern through symmetric channel. He demonstrated through asymptotic analysis that both the cyclic peristaltic contractions of the fallopian tube/oviduct wall and the swaying motions of the cilia tips which lined the interior surfaces of the oviduct work together while transporting the embryo. He concluded that the ciliary propulsion can be an important factor for the motion of fluid, although it is of smaller amplitude than the peristaltic waves.

Motivated from the literature[1–15,26–29], for the first time, we develop a two-dimensional mathematical model to theoretically assess the peristaltic-ciliary transport of a developing embryo within a fallopian tubal fluid in the human fallopian tube. In the current model, we propose a finite two-dimensional narrow tube which has cyclic peristaltic contractions and its inner surface is lined with a layer of mucus membrane. The mucus membrane of the tube is crowded with secretory and ciliated cells of different heights. The cyclic peristaltic contractions generate sinusoidal wave, and swaying motions of the cilia tips generate metachronal wave. The secretory cells pour out a small volume of the fallopian tubal fluid. The sinusoidal wave and the metachronal wave merge together to generate a travelling wave that in turn drives the linearly viscous fluid within a fallopian tubal fluid through the fallopian tube, from the ampulla to the intramural of the fallopian tube. We derive the expressions for the axial and radial velocities, the appropriate residue time over wavelength, the stream function, the pressure gradient, the pressure difference over wavelength, the volume flow rate, and the time mean volume flow rate. Through graphs and table, we provide an estimation of the quantitative effects of various parameters and constants involved in the present analysis. Relevance of the results of current assessment to the transport of a developing embryo within a fallopian tubal fluid from the ampulla to the intramural in the fallopian tube is also explored.

The rest of the paper is organized as follows. Section 2 contains the mathematical formulation of the problem, the governing equations of motion, and the solution to the resulting partial differential equation, and includes expressions for the important physical quantities such as the appropriate residue time over wavelength t_{r}, the pressure gradient $\mathrm{d}_z p$, the pressure difference over wavelength Δp_λ, the stream function ψ, the volume flow rate q, and the time mean volume flow rate Q_T in the moving frame of reference. Effects of the pressure gradient at the tube entrance ξ, the metachronal wave parameter ϵ, and the amplitude ratio ϕ are discussed through graphs and table in Section 3. Concluding remarks are given in Section 4.

2 Mathematical formulation and solution

We consider the peristaltic-ciliary transport of a developing embryo within a fallopian tubal fluid in the human fallopian tube. As a model, we examine the flow of an incompressible linearly viscous fluid in a finite two-dimensional narrow tube of mean radius r_{t}. The schematic diagrams of the finite narrow tube and human fallopian tube are shown in Figs. 1 and 2, respectively. In Fig. 1, a cylindrical coordinate system is chosen, in which the $\overline{Z}$-axis is taken along the tube, and the $\overline{R}$-axis is normal to the tube in the upward direction.

We assume that the tube surface has cyclic peristaltic contractions and the inner surface of the tube is lined with a layer of mucus membrane. The mucus membrane is crowded with secretory and ciliated cells. The secretory cells pour out a small volume of fallopian tubal fluid. The ciliated cells, which are of different heights, form hair like structures. Both the cyclic peristaltic contractions and the swaying motions of the cilia tips are in continuum and work

together to generate a travelling wave of the form

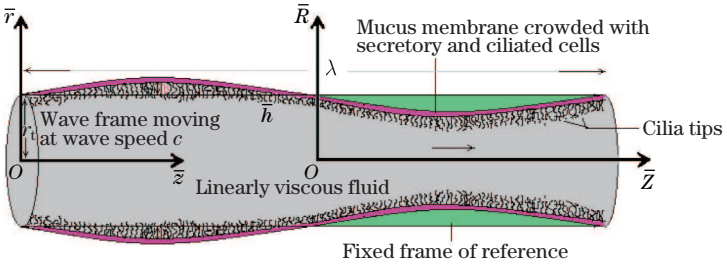

Fig. 1 Schematic diagram of the finite narrow tube

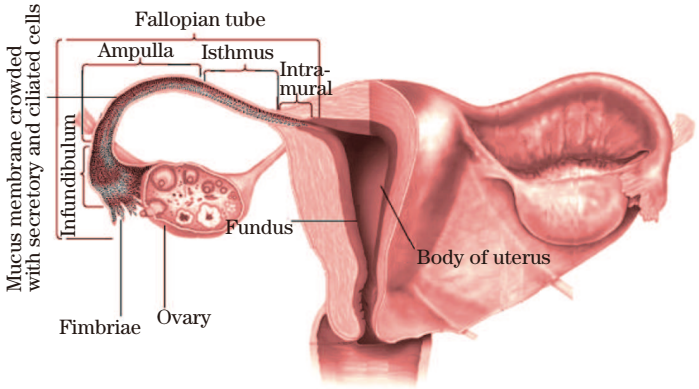

Fig. 2 Schematic diagram of the human fallopian tube

$$\overline{H}(\overline{Z},\overline{t}) = r_{\mathrm{t}} + \overline{F}(\overline{Z},\overline{t}) + \overline{G}(\overline{Z},\overline{t}), \tag{1}$$

where $\overline{F}(\overline{Z},\overline{t})$ can be viewed as the underlying cyclic peristaltic contractions that generate sinusoidal wave propagating at a wave speed c with different amplitudes,

$$\overline{F}(\overline{Z},\overline{t}) = b\sin\Big(\frac{2\pi}{\lambda}(\overline{Z} - c\overline{t})\Big), \tag{2}$$

in which b is the amplitude of the sinusoidal wave, λ is the wavelength, and $\overline{t}$ is any instant of time[16–25]. $\overline{G}(\overline{Z},\overline{t})$ can be thought as the effects of swaying motions of the cilia tips that generate metachronal wave. The metachronal wave propagates in an elliptical path, in the form of an envelope at a wave speed c with different amplitudes,

$$\overline{G}(\overline{Z},\overline{t}) = Ab\frac{2\pi}{\lambda}\cos\Big(\frac{2\pi}{\lambda}(\kappa(\overline{Z} - c\overline{t}))\Big)\sin\Big(\frac{2\pi}{\lambda}(\overline{Z} - c\overline{t})\Big), \tag{3}$$

where Ab is the maximum displacement of the material points, κ is the constant, and A is the amplitude of the metachronal wave of cilia[13–15]. Logical basis behind the formulation of travelling wave (1) is drawn from the biological contexts of the human fallopian tube[1–3,6–13].

We choose the origin at the midplane so that $-r_{\mathrm{t}} \leqslant \overline{R} \leqslant r_{\mathrm{t}}$. We further assume the fallopian tubal fluid as an incompressible linearly viscous fluid and consider that the linearly viscous fluid within a fallopian tubal fluid fills the tube. The travelling wave (1) propagates along the surface of tube at a wave speed c and drives the linearly viscous fluid within a fallopian tubal fluid.

Now, we introduce a moving frame of reference $(\overline{r},\overline{z})$ at a wave speed c, in which the flow of the linearly viscous fluid within the fallopian tubal fluid becomes independent of time $\overline{t}$. The

coordinates $\overline{R}$ and $\overline{Z}$, the components of the velocity $\overline{U}$ and $\overline{W}$, the travelling wave $\overline{H}$, and the pressure $\overline{P}$ in the laboratory frame the of reference are related with the moving frame of reference coordinates $\overline{r}$ and $\overline{z}$, the components of the velocity $\overline{u}$ and $\overline{w}$, the travelling wave $\overline{h}$, and the pressure $\overline{p}$ through the following relations:

$$\begin{cases} \overline{Z} = \overline{z} + c\overline{t}, \quad \overline{R} = \overline{r}, \\ \overline{W}(\overline{R}, \overline{Z}, \overline{t}) = \overline{w}(\overline{r}, \overline{z}) + c, \quad \overline{U}(\overline{R}, \overline{Z}, \overline{t}) = \overline{u}(\overline{r}, \overline{z}), \\ \overline{H}(\overline{Z}, \overline{t}) = \overline{h}(\overline{z}), \quad \overline{P}(\overline{Z}, \overline{t}) = \overline{p}(\overline{z}), \end{cases} \tag{4}$$

and scale the following dimensionless parameters:

$$r = \frac{\overline{r}}{r_{\mathrm{t}}}, \quad z = \frac{\overline{z}2\pi}{\lambda}, \quad u = \frac{\overline{u}\lambda}{2\pi c r_{\mathrm{t}}}, \quad w = \frac{\overline{w}}{c}, \quad p = \frac{\overline{p}2\pi r_{\mathrm{t}}^2}{\mu\lambda c}, \quad h = \frac{\overline{h}}{r_{\mathrm{t}}}.$$

The basic equations that govern the two-dimensional flow of an incompressible linearly viscous fluid neglecting the thermal effects and in the absence of body force in the moving frame of reference, in a dimensionless form, are given by

$$\partial_r(ru) = -r\partial_z w, \tag{5}$$

$$\alpha^3 Re(u\partial_r + w\partial_z)u = -\partial_r p + \alpha^2\partial_r(r^{-1}\partial_r(ru)) + \alpha^4\partial_{z^2}^2 u, \tag{6}$$

$$\alpha Re(u\partial_r + w\partial_z)v = -\partial_z p + r^{-1}\partial_r(r\partial_r w) + \alpha^2\partial_{z^2}^2 w, \tag{7}$$

where ∂_r and ∂_z denote the partial derivatives with respect to r and z, respectively, while $\alpha = \frac{2\pi r_{\mathrm{t}}}{\lambda}$ is the wave number, and $Re = \frac{c r_{\mathrm{t}}}{\nu}$ is the Reynolds number. The travelling wave (1) after utilizing the transformations defined in Eq. (4) and scaled dimensionless parameters yields

$$h(z) = 1 + \phi\sin z + \epsilon\phi\cos(\kappa z)\sin z, \tag{8}$$

in which $\phi = \frac{b}{r_{\mathrm{t}}}$ is the amplitude ratio, and $\epsilon = \frac{2\pi A}{\lambda}$ is the metachronal wave parameter. Equation (8) represents the travelling wave of tube surface in the moving fame of reference, in a dimensionless form.

The dimensionless boundary conditions, associated with Eqs. (6) and (7), in the moving frame of reference are

$$u(0, z) = 0, \quad u(h, z) = -\mathrm{d}_z h, \tag{9}$$

$$\partial_r w(0, z) = 0, \quad w(h, z) = -1, \tag{10}$$

in which d_z denotes the material derivative with respect to z. Further to apply the lubrication theory to the peristaltic-ciliary flow, we assume Re of the order of 0.001 and the wavelength λ of the travelling wave to be large relative to the radius of the tube r_{t}, i.e., $\frac{r_{\mathrm{t}}}{\lambda} \ll 1$[10,16–17]. After employing these assumptions, Eqs. (6) and (7) become

$$\partial_r p = 0, \tag{11}$$

$$\partial_z p = r^{-1}\partial_r(r\partial_r w). \tag{12}$$

From Eq. (11), we infer that $p = p(z)$ only. Therefore, Eq. (11) becomes

$$\partial_r(r\partial_r w) = r\mathrm{d}_z p. \tag{13}$$

Integrating Eq. (13) twice with respect to r and then in turn using its boundary conditions (10), one acquires

$$w(r, z) = -\frac{\mathrm{d}_z p}{4}((1 + \phi\sin z + \epsilon\phi\cos(\kappa z)\sin z)^2 - r^2) - 1, \tag{14}$$

which is the axial velocity of the peristaltic-ciliary flow of linearly viscous fluid within a fallopian tubal fluid.

We suppose that mitotic divisions take place in the linearly viscous fluid within a fallopian tubal fluid during the peristaltic-ciliary flow[5]. Proper and complete mitotic divisions occur for appropriate residue time[30–31]. The appropriate residue time over wavelength t_{r} in a dimensionless form is defined as

$$t_{\mathrm{r}} = \int_0^{2\pi} \frac{1}{w(r,z)} \mathrm{d}z, \tag{15}$$

in which the variable r is to be kept fixed during the integration and $t_{\mathrm{r}} = \frac{2\pi c \bar{t}_{\mathrm{r}}}{\lambda}$. Equation (15) with the help of Eq. (14) provides the appropriate residue time over wavelength at which proper and complete mitotic divisions occur.

Substitution of Eq. (14) into Eq. (5), in turn the integration of the resulting partial differential equation with respect to r and then after making use of the boundary condition (9) for $r = 0$, one gets the radial velocity of the peristaltic-ciliary flow of linearly viscous fluid within a fallopian tubal fluid,

$$\begin{aligned} u(r,z) =& \frac{\mathrm{d}^2_{z^2} p}{16}(2(1+\phi\sin z+\epsilon\phi\cos(\kappa z)\sin z)^2 r - r^3) \\ &+ \frac{\mathrm{d}_z p}{4}((\phi+\phi^2(1+\epsilon\cos(\kappa z))\sin z)(\cos z+\epsilon\cos z\cos(\kappa z) \\ &- \kappa\epsilon\sin z\sin(\kappa z))r). \end{aligned} \tag{16}$$

Using the boundary condition (9) for $r = h$ in Eq. (16) and then solving the resultant equation for the pressure gradient $\mathrm{d}_z p$, we get

$$\mathrm{d}_z p = -\frac{(8(1+\phi\sin z+\epsilon\phi\cos(\kappa z)\sin z)^2 + 16B_0)}{(1+\phi\sin z+\epsilon\phi\cos(\kappa z)\sin z)^4}, \tag{17}$$

in which B_0 is an arbitrary constant to be determined, related to the pressure gradient at the entrance of tube. Using $\frac{\mathrm{d}p(0)}{\mathrm{d}z} = -\xi$ (in which ξ is the constant, denoting the pressure gradient at the tube entrance) into Eq. (17), we have

$$\mathrm{d}_z p = -\frac{(8(1+\phi\sin z+\epsilon\phi\cos(\kappa z)\sin z)^2 + \xi - 8)}{(1+\phi\sin z+\epsilon\phi\cos(\kappa z)\sin z)^4}, \tag{18}$$

which is the expression for the pressure gradient of the peristaltic-ciliary flow of linearly viscous fluid within a fallopian tubal fluid. The pressure difference over wavelength Δp_λ in a dimensionless form is defined as

$$\Delta p_\lambda = \int_0^{2\pi} \mathrm{d}_z p \mathrm{d}z, \tag{19}$$

which upon using Eq. (18) provides the pressure difference Δp_λ over wavelength. Introduction of dimensionless stream function ψ in the moving frame of reference

$$u(r,z) = -r^{-1}\partial_z\psi, \quad w(r,z) = r^{-1}\partial_r\psi$$

into Eq. (16) yields

$$\psi(r,z) = -\frac{1}{16}\mathrm{d}_z p\big(2(1+\phi\sin z+\epsilon\phi\cos(\kappa z)\sin z)^2 r^2 - r^4\big) + C_1(r), \tag{20}$$

where $C_1(r)$ is an arbitrary function to be determined. Since the midplane of the tube is also streamlined in the moving frame of reference, by convention we may choose the zero value of the streamline at the midplane[16], i.e.,

$$\psi(0,z) = 0. \tag{21}$$

Substitution of Eq. (21) into Eq. (20) yields

$$\psi(r,z) = -\frac{1}{16}\mathrm{d}_z p\big(2(1+\phi\sin z+\epsilon\phi\cos(\kappa z)\sin z)^2 r^2 - r^4\big). \tag{22}$$

The dimensionless instantaneous volume flow rate in the laboratory frame of reference is defined as

$$Q = \int_0^H W(R,Z,t)R\mathrm{d}R, \tag{23}$$

where $R=\frac{\overline{R}}{r_{\mathrm{t}}}$, $Z=\frac{2\pi\overline{Z}}{\lambda}$, $t=\frac{2\pi c\overline{t}}{\lambda}$, $W=\frac{\overline{W}}{c}$, and $H=\frac{\overline{H}}{r_{\mathrm{t}}}$. In Eq. (23), the variables Z and t are to be held fixed during the integration.

In a dimensionless form, the coordinates, the axial velocities, and the travelling waves in the laboratory frame of reference and the moving frame of reference are related through

$$\begin{cases} Z = z+t, \quad R = r, \\ W(R,Z,t) = w(r,z)+1, \quad H(Z,t) = h(z). \end{cases} \tag{24}$$

Substituting the relation (24) into Eq. (23) yields

$$Q = q + \frac{h^2}{2}, \tag{25}$$

where

$$q = \int_0^h w(r,z)r\mathrm{d}r, \tag{26}$$

which is the volume flow rate in a dimensionless form, in the moving frame of reference. In Eq. (26), z is to be kept fixed during the integration. Equation (25) relates the instantaneous volume flow rate in the laboratory frame of reference with the volume flow rate in the moving frame of reference.

The time mean volume flow rate over a period T of the travelling wave in the laboratory frame of reference, in a dimensionless form is defined as

$$Q_T = \frac{1}{T}\int_0^T Q\mathrm{d}t. \tag{27}$$

From Eq. (26), it is delineated that q is independent of time t. Therefore, Eq. (27) after making use of Eqs. (25) and (26) provides

$$Q_T = q + \frac{1}{2}\int_0^1 h^2\mathrm{d}z. \tag{28}$$

Equation (28) upon utilizing Eq. (8) gives rise to

$$Q_T = q + 0.5 + 0.46\phi + 0.14\phi^2 + \frac{\epsilon^2\phi^2 K_1}{32} + \frac{\epsilon\phi^2 K_2}{\kappa(\kappa^2-4)} + \frac{\epsilon\phi K_3}{\kappa^2-1}, \tag{29}$$

where

$$\begin{aligned} K_1 &= 2.18 + \frac{\sin(2-2\kappa)}{\kappa-1} + \frac{2\sin 2\kappa}{\kappa} - \frac{\sin(2(\kappa+1))}{\kappa+1}, \\ K_2 &= 0.91\kappa\cos\kappa - (2-0.71\kappa^2)\sin\kappa, \\ K_3 &= 0.54\cos\kappa + 0.84\kappa\sin\kappa - 1. \end{aligned}$$

Equation (26) in terms of the stream function ψ is given by

$$q = \int_0^h \partial_r \psi \mathrm{d}r, \tag{30}$$

which in turn using the boundary condition (21) and Eq. (22) at $r = h$ yields

$$q = -\frac{\mathrm{d}_z p}{16}(1 + \phi \sin z + \epsilon\phi \cos(\kappa z) \sin z)^4. \tag{31}$$

3 Results and discussion

The peristalsis-cilia induced flow of linearly viscous fluid within a fallopian tubal fluid in a finite two-dimensional narrow tube is established in the previous section. We choose $r_{\mathrm{t}} = 1.0$ and $L = 2\lambda$ (where $\lambda = 2\pi$), respectively, as the averaged values for the mean radius and the length of the tube. The present model considers a geometry that represents averaged values of a sagittal cross section of the human fallopian tube. In the geometry, three regions of the fallopian tube: ampullar, isthmus, and intramural, are considered. At the entrance of the ampullar region, the ovum enters with the pressure gradient $-\xi$. The ovum and the spermatozoon fuse to become an embryo. The developing embryo within a fallopian tubal fluid is then transported by the travelling wave from ampulla to intramural, in the fallopian tube. The axial w and radial u velocities, the residue time over wavelength t_{r}, the pressure difference over wavelength Δp_λ, the stream function ψ, the volume flow rate q, and the time mean volume flow rate Q_T are the flow variables that characterize the peristaltic-ciliary transport of a developing embryo within the fallopian tube. By employing the lubrication approximation theory in the moving frame of reference, the expressions for the aforesaid flow variables are derived.

This section presents an estimation of the quantitative effects of pressure gradient at the tube entrance ξ, the metachronal wave parameter ϵ, and the amplitude ratio ϕ on the axial w and radial u velocities, the residue time over wavelength t_{r}, the volume flow rate q, the pressure difference over wavelength Δp_λ, and the stream function ψ through graphs and the axial velocity w through table . We perform numerical integration for the appropriate residue time over wavelength t_{r} and the pressure difference over wavelength Δp_λ in MATHEMATICA.

We choose one sagittal cross section $\left(r, \frac{4\pi}{3}\right)$ and one frontal cross section $(0.3,\ z)$ to observe the quantitative effects of the pressure gradient at the tube entrance ξ, the metachronal wave parameter ϵ, and the amplitude ratio ϕ on the distribution of axial velocity, respectively along the radial distance and the axial distance.

Table 1 provides the distribution of axial velocity along the radial distance for both cases, i.e., the peristaltic flow (when $\epsilon = 0.00$) and the peristaltic-ciliary flow (when $\epsilon = 0.15$) at the sagittal cross section $\left(r, \frac{4\pi}{3}\right)$. It is noted from this table that the axial velocity is the maximal at the midplane of tube and the minimal near the tube surface. The axial velocity of the peristaltic-ciliary flow is lesser than that of the peristaltic flow. This is because of the inclusion of swaying motions of the cilia tips that work along with the cyclic peristaltic contractions of the tube surface. In other words, one may say that, the inclusion of cilia causes reduction in the axial velocity along the radial distance. Negative sign is the clear indication of backward flow near the tube surface.

Table 1 Distribution of the axial velocity along the radial distance when $\phi = 0.13$, $\xi = 7.0$, and $\kappa = 1.5$

r	Peristaltic flow $\epsilon = 0.00$	Peristaltic-ciliary flow $\epsilon = 0.15$
	$w(r, \frac{4\pi}{3})$	$w(r, \frac{4\pi}{3})$
−1.00	−1.453 546	−1.533 725
−0.50	0.148 408	0.119 154
0.00	0.682 543	0.670 107
0.50	0.148 408	0.119 154
1.00	−1.453 546	−1.533 725

Figure 3 shows the distribution of the axial velocity along the radial distance at the sagittal cross section $\left(r, \frac{4\pi}{3}\right)$. It is seen from Fig. 3 that due to no-slip condition, the axial velocity profiles are parabolic in nature across the tube diameter. Figures 3(a)–3(c) display the effects of the pressure gradient at the tube entrance ξ, the metachronal wave parameter ϵ, and the amplitude ratio on the radial distribution of axial velocity. The axial velocity increases radially with an increase in ξ as is depicted through Fig. 3(a). From Figs. 3(b) and 3(c), it is noted that the axial velocity decreases radially with the increment in ϵ and ϕ. The pressure gradient at the tube entrance ξ plays a vital role in the flow of peristaltic-ciliary flow of linearly viscous fluid within a fallopian tubal fluid. We plot Fig. 3(d) to check the limit for ξ with $\epsilon = 0.08$, $\phi = 0.13$, and $k = 1.5$. It is disclosed from this figure that, when $\xi > 1.85$, the flow is in the forward direction, and when $\xi < 1.85$, the flow is in the backward direction. At $\xi = 1.85$, the axial velocity profile shows linear relation between r and $w\left(r, \frac{4\pi}{3}\right)$. Comparison between the radial distribution of axial velocity of the peristaltic flow (when $\epsilon = 0.00$) and the peristaltic-ciliary flow (when $\epsilon = 0.15$) is made in Fig. 3(e). Along the radial distance, the peristaltic flow has a larger axial velocity as compared with the peristaltic-ciliary flow.

The amplitude ratio $\left(\phi = \frac{b}{a}\right)$ is the ratio of b (amplitude of the sinusoidal wave of the tube surface peristaltic contractions) to r_{t} (mean radius of the tube). Since we choose $r_{\mathrm{t}} = 1.0$, an increase in ϕ means an increase in b. The axial velocity decreases radially when b increases. The metachronal wave parameter $\left(\epsilon = \frac{2\pi A}{\lambda}\right)$ is the ratio of A (amplitude of the metachronal wave of cilia) to λ (wavelength of the travelling wave of the tube surface). Since we take $\lambda = 2\pi$, an increase in ϵ means an increase in A. The axial velocity decreases radially as A is incremented. This decrease in the axial velocity is the clear evidence of the noticeable impact of swaying motions of the cilia tips on the axial velocity. Furthermore, one may reveal that, when the sinusoidal wave of larger amplitude and the metachronal wave of larger amplitude merge together to form a travelling wave of lager amplitude, slowness in the flow in the direction of propagation of the travelling wave of tube surface happens.

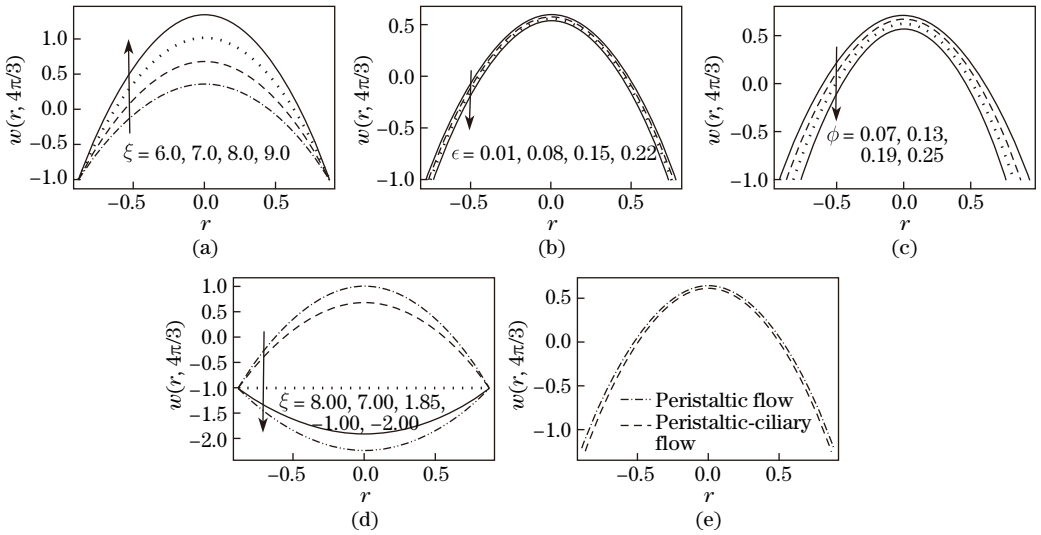

Fig. 3 Axial velocity versus radial distance profiles when there are variations in (a) pressure gradient at the tube entrance ξ (when $\epsilon = 0.08$, $\phi = 0.13$, and $k = 1.5$), (b) metachronal wave parameter ϵ (when $\phi = 0.25$, $\xi = 7.0$, and $k = 1.5$), and (c) amplitude ratio ϕ (when $\epsilon = 0.08$, $\xi = 7.0$, and $k = 1.5$), (d) limit for the pressure gradient at the tube entrance ξ (when $\epsilon = 0.08$, $\phi = 0.13$, and $k = 1.5$), and (e) comparison between the peristaltic flow and the peristaltic-ciliary flow (when $\xi = 7.0$, $\phi = 0.19$, and $k = 1.5$) at the sagittal cross section $\left(r, \frac{4\pi}{3}\right)$

Figure 4 provides the distribution of axial velocity along the axial distance at the frontal

cross section $(0.3,\ z)$. Through Figs. 4(a)–4(c), we observe effects of the pressure gradient at the tube entrance ξ, the metachronal wave parameter ϵ, and the amplitude ratio ϕ on the axial distribution of axial velocity. It is noted from Fig. 4(a) that the axial velocity enhances axially as ξ is increased. In Fig. 4(b), we divide the axial distance (tube length) $2\lambda = [0, 4\pi]$ into 8 subintervals $\left[0, \frac{\pi}{3}\right]$, $\left[\frac{\pi}{3}, \frac{13\pi}{12}\right]$, $\left[\frac{13\pi}{12}, \frac{7\pi}{4}\right]$, $\left[\frac{7\pi}{4}, \frac{25\pi}{12}\right]$, $\left[\frac{25\pi}{12}, \frac{29\pi}{12}\right]$, $\left[\frac{29\pi}{12}, \frac{19\pi}{6}\right]$, $\left[\frac{19\pi}{6}, \frac{23\pi}{6}\right]$, and $\left[\frac{23\pi}{6}, 4\pi\right]$ to observe properly the effects of ϵ on the axial distribution of axial velocity. The axial velocity increases axially within the subintervals $\left[0, \frac{\pi}{3}\right]$, $\left[\frac{7\pi}{4}, \frac{25\pi}{12}\right]$, $\left[\frac{29\pi}{12}, \frac{19\pi}{6}\right]$, and $[\frac{19\pi}{6}, \frac{23\pi}{6}]$, while it decreases axially within the subintervals $\left[\frac{\pi}{3}, \frac{13\pi}{12}\right]$, $\left[\frac{13\pi}{12}, \frac{7\pi}{4}\right]$, $\left[\frac{25\pi}{12}, \frac{29\pi}{12}\right]$, and $\left[\frac{23\pi}{6}, 4\pi\right]$ with an increase in ϵ. It is also evident from the peak to peak value deviations in the axial velocity versus axial distance profile comparison that the axial velocity decreases axially during the first wavelength and increases axially during the second wavelength when ϵ increases. To properly delineate the effects of ϕ on the axial distribution of axial velocity, we divide the tube length in Fig. 4(c) into four subintervals $[0, \pi]$, $[\pi, \frac{25\pi}{12}]$, $[\frac{25\pi}{12}, \frac{19\pi}{6}]$, and $[\frac{19\pi}{6}, 4\pi]$. The axial velocity decreases axially within the subintervals $[\pi, \frac{25\pi}{12}]$ and $[\frac{19\pi}{6}, 4\pi]$, whereas it increases axially within the subintervals $[0, \pi]$ and $[\frac{25\pi}{12}, \frac{19\pi}{6}]$ with the increment in ϕ. We disclose from the peak to peak value deviation comparison of the axial velocity versus axial distance profiles that the axial velocity increases axially by increasing ϕ. Figure 4(d) provides comparison between the axial distribution of axial velocity of the peristaltic flow (when $\epsilon = 0.00$) and the peristaltic-ciliary flow (when $\epsilon = 0.15$). It is evident from the peak to peak value deviation comparison of the axial velocity versus axial distance profiles that the axial velocity of the peristaltic-ciliary flow is smaller as compared with the peristaltic flow during the first wavelength and larger during the second wavelength.

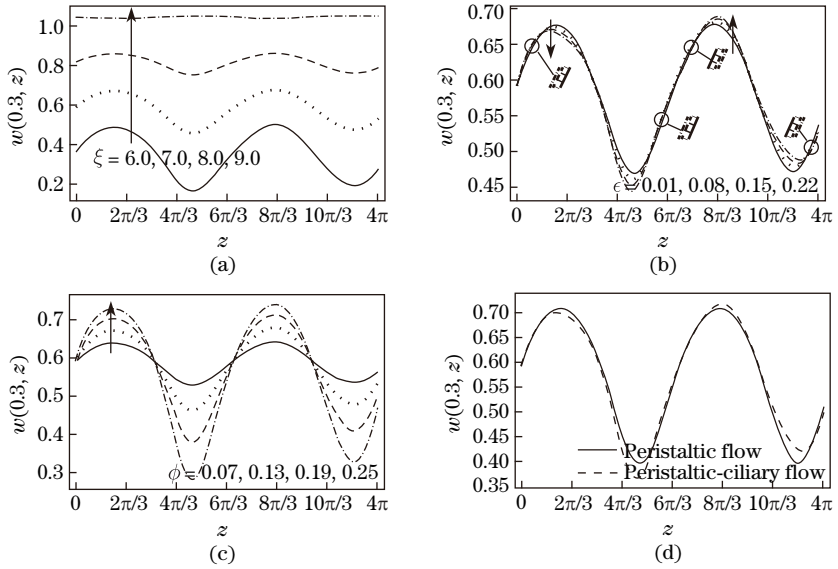

Fig. 4 Axial velocity versus axial distance profiles when there are variations in (a) pressure gradient at the tube entrance ξ (when $\epsilon = 0.08$, $\phi = 0.13$, and $k = 1.5$), (b) metachronal wave parameter ϵ (when $\phi = 0.13$, $\xi = 7.0$, and $k = 1.5$), and (c) amplitude ratio ϕ (when $\epsilon = 0.08$, $\xi = 7.0$, and $k = 1.5$) and (d) comparison between the peristaltic flow and the peristaltic-ciliary flow (when $\xi = 7.0$, $\phi = 0.19$, and $k = 1.5$) at the frontal cross section $(0.3, z)$

In Fig. 5, vector plots are plotted to observe the local flow behavior of peristaltic-ciliary flow of linearly viscous fluid within a fallopian tubal fluid. Effects of the pressure gradient at the tube entrance ξ, the metachronal wave parameter ϵ, and the amplitude ratio ϕ can easily be seen through Fig. 5. Comparison between the flow behavior of the peristaltic flow and the

peristaltic-ciliary flow is made in Figs. 5(m) and 5(n). A backward flow near the tube surface is also evident from these vector plots.

Figure 6 is prepared to inspect the behavior of the pressure gradient at the tube entrance ξ, the metachronal wave parameter ϵ, and the amplitude ratio ϕ on the appropriate residue time over wavelength at the frontal cross section $(0.3, z)$. It is inferred from Fig. 6(a) that an increment in ξ results in a decrease in the appropriate residue time over wavelength. This outcome is consistent with the fact that the more pressure gradient at the tube entrance, the

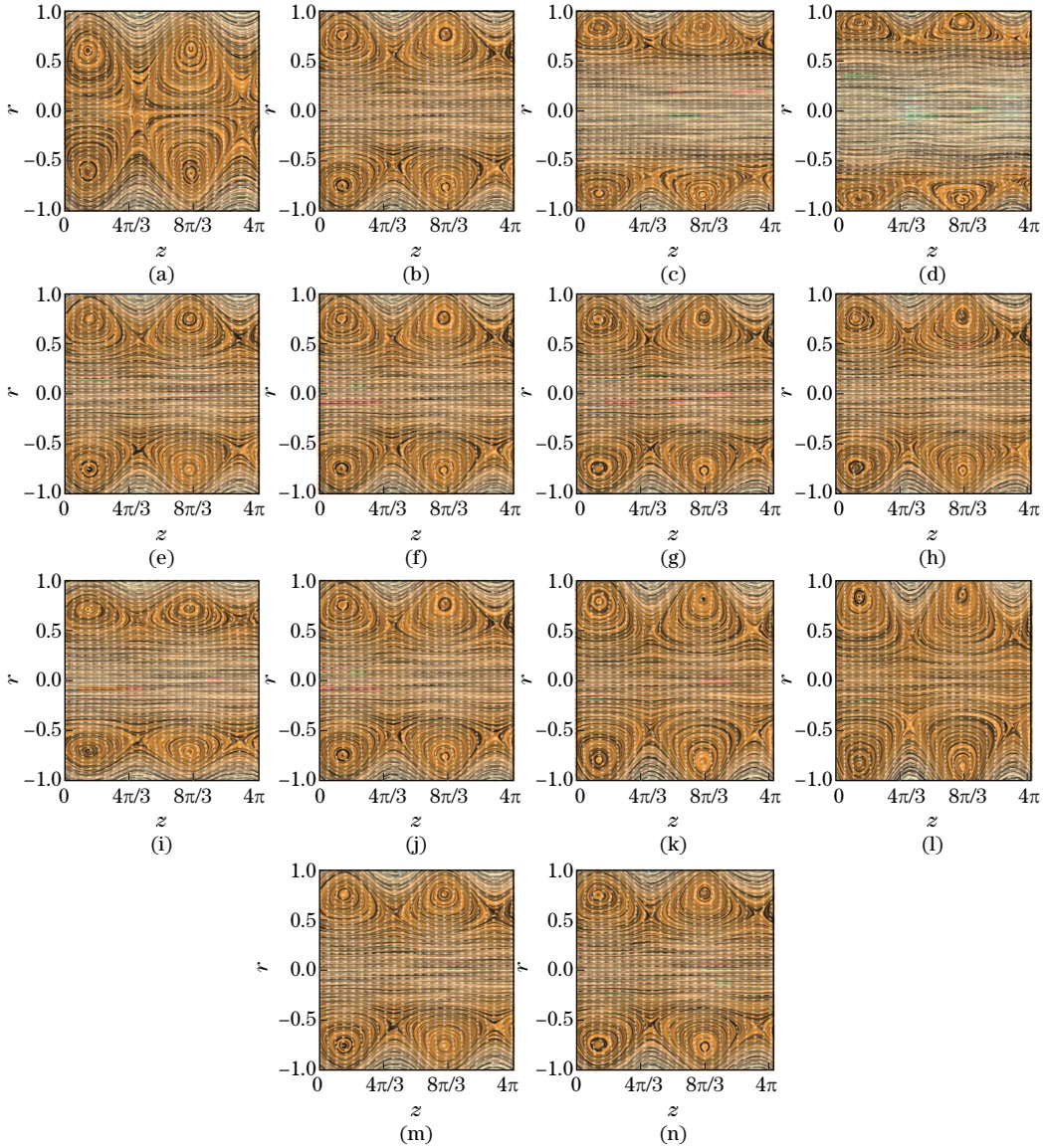

Fig. 5 Vector plots depicting the local flow behavior when there are various pressure gradients at the tube entrance ((a) $\xi = 5.0$, (b) $\xi = 7.0$, (c) $\xi = 9.0$, and (d) $\xi = 11.0$) when $\epsilon = 0.08$, $\phi = 0.13$, and $k = 1.5$, when there are various metachronal wave parameters ((e) $\epsilon = 0.01$, (f) $\epsilon = 0.08$, (g) $\epsilon = 0.15$, and (h) $\epsilon = 0.22$) when $\xi = 7.0$, $\phi = 0.13$, and $k = 1.5$, and when there are various amplitude ratios ((i) $\phi = 0.07$, (j) $\phi = 0.13$, (k) $\phi = 0.19$, and (l) $\phi = 0.25$) when $\xi = 7.0$, $\epsilon = 0.08$, and $k = 1.5$, and comparison between (m) peristaltic flow and (n) peristaltic-ciliary flow when $\xi = 7.0$, $\phi = 0.19$, and $k = 1.5$

lesser appropriate residue time over wavelength. Figures 6(b) and 6(c) delineate that as we increase the values of ϵ and ϕ, the appropriate residue time over wavelength increases. More specifically, one may relate this increase in the appropriate residue time over wavelength with amplitudes of the sinusoidal wave and the metachronal wave, respectively. The appropriate residue time over wavelength increases as the amplitudes of both the sinusoidal and metachronal waves are incremented. It means that the residue time increases as the wave progresses with larger amplitudes. Figure 6(d) describes a comparison between the appropriate residue time over wavelength of the peristaltic flow (when $\epsilon = 0.00$) and the peristaltic-ciliary flow (when $\epsilon = 0.15$) of linearly viscous fluid within a fallopian tubal fluid. This comparison enables us to infer that, the peristaltic-ciliary flow has more appropriate residue time over wavelength than the peristaltic flow.

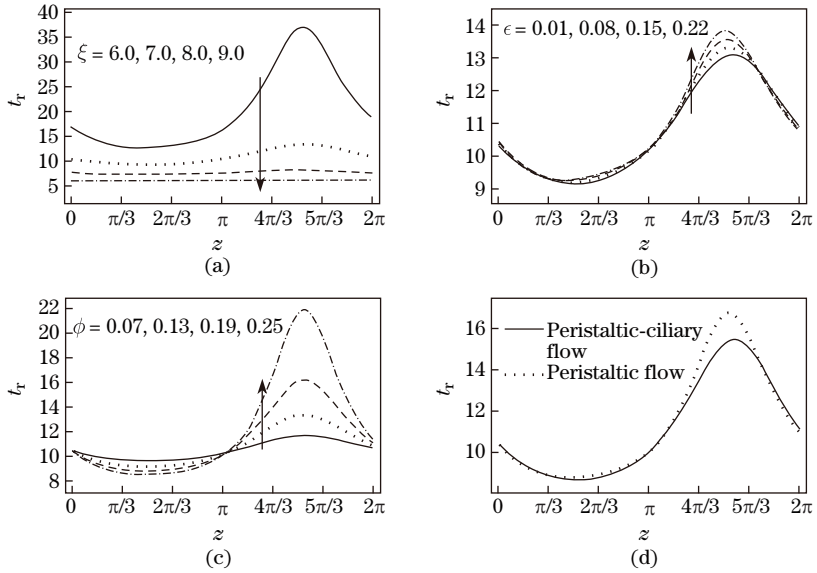

Fig. 6 Appropriate residue time over wavelength versus axial distance profiles when there are variations in (a) pressure gradient at the tube entrance ξ when $\epsilon = 0.08$, $\phi = 0.13$, and $k = 1.5$, (b) metachronal wave parameter ϵ when $\phi = 0.13$, $\xi = 7.0$, and $k = 1.5$, and (c) amplitude ratio ϕ when $\epsilon = 0.08$, $\xi = 7.0$, and $k = 1.5$, and (d) comparison between the peristaltic flow and the peristaltic-ciliary flow (when $\xi = 7.0$, $\phi = 0.13$, $k = 1.5$, and $r = 0.5$) at the frontal cross section $(0.3, z)$

Proper and complete mitotic divisions during the peristaltic-ciliary flow take place in the linearly viscous fluid for the appropriate residue time over wavelength. Probability of the proper and complete mitotic divisions increases in turn with an increase in the appropriate residue time over wavelength. By controlling the value of pressure gradient at the tube entrance and amplitudes of both the sinusoidal and metachronal waves by some biomechanical means, one can control the appropriate residue time to get the proper, complete, and all required mitotic divisions. In Fig. 7, a complete process of mitotic divisions, that takes place in the developing embryo transport from ampulla to intramural in the fallopian tube, is shown.

Figure 8 corresponds to effects of the pressure gradient at the tube entrance ξ, the metachronal wave parameter ϵ, and the amplitude ratio ϕ on the volume flow rate. Figure 8(a) depicts that the volume flow rate decreases for any particular value of ϵ when ϕ increases, while it decreases with an increase in ϵ. It is speculated from Fig. 8(b) that the volume flow rate reduces for any individual value of ξ as ϵ is incremented, whereas it enhances with the increment in ξ. Analogy of the volume flow rate between the peristaltic flow (when $\epsilon = 0.00$) and the peristaltic-ciliary flow (when $\epsilon = 0.15$) is elaborated in Fig. 8(c). This figure delineates that the peristaltic flow has more volume flow rate as compared with the peristaltic-ciliary flow.

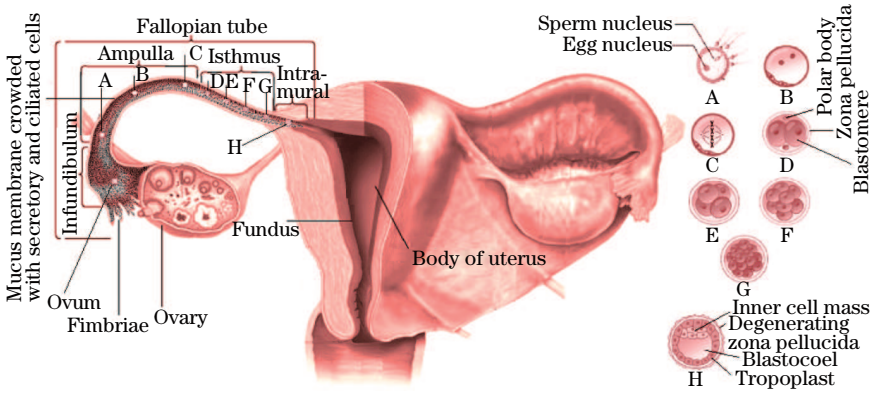

Fig. 7 (A) A sperm penetrates the ovum cytoplasm, activating the ovum, extrudes a second polar body, and forms the female pronucleus. (B) The sperm pronucleus is released into the ovum cytoplasm, after which the two pronuclei fuse. (C) Mingling of male and female chromosomes, replication and division of the chromosomes. (D)–(G) The embryo then undergoes successive mitotic divisions to produce a morula (G). (H) An early blastocyst (a fluid filled cavity)[5]

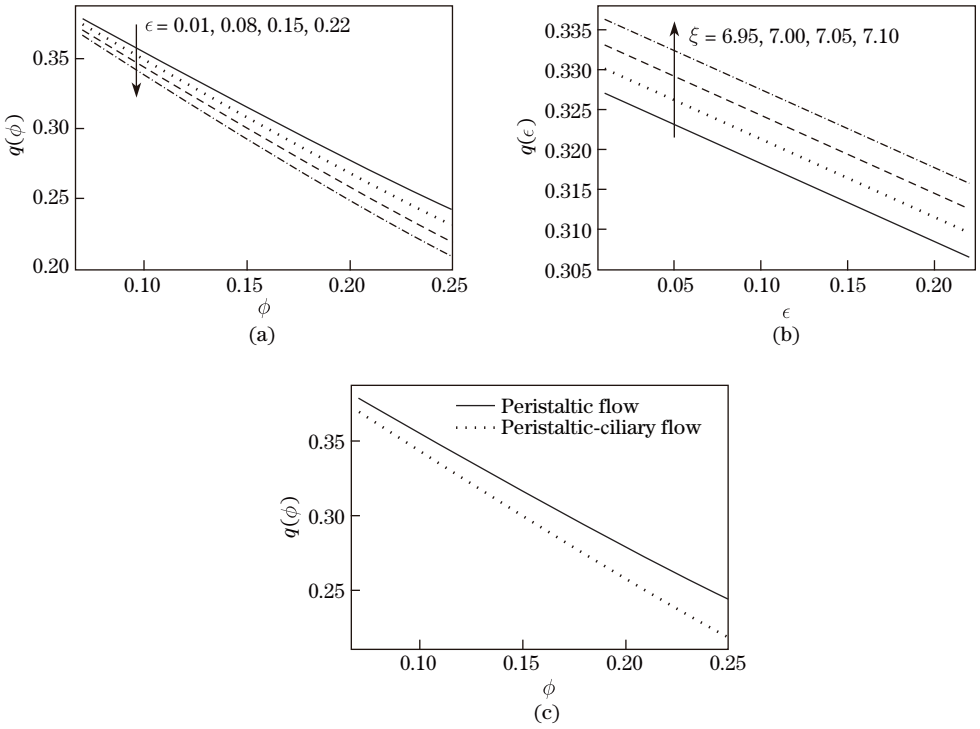

Fig. 8 Volume flow rate versus (a) amplitude ratio profiles when there are various metachronal wave parameter ϵ (when $\xi = 7.00$, $\kappa = 1.5$, and $z = \frac{4\pi}{3}$) and (b) metachronal wave parameter profiles when there are various pressure gradient at the tube entrance ξ (when $\phi = 0.13$, $\kappa = 1.5$, and $z = \frac{4\pi}{3}$), and (c) amplitude ratio profiles for comparison between peristaltic flow and peristaltic-ciliary flow (when $\xi = 7.00$, $\kappa = 1.5$, and $z = \frac{4\pi}{3}$)

Figure 9 is displayed to analyze the pumping characteristics of the peristaltic-ciliary flow of linearly viscous fluid within a fallopian tubal fluid. A linear relation between Δp_λ and Q_T is observed in these profiles. The pressure difference over wavelength versus time mean volume flow rate plane is divided into four conventional quadrants. The quadrant I denotes the peristaltic-ciliary pumping region (when $Q_T > 0$ and $\Delta p_\lambda > 0$), the quadrant II represents the

retrograde pumping region (when $Q_T < 0$ and $\Delta p_\lambda > 0$), in the quadrant III (when $Q_T < 0$ and $\Delta p_\lambda < 0$), no flow takes place, and the quadrant IV defines the augmented pumping region (when $Q_T > 0$ and $\Delta p_\lambda < 0$). In the peristaltic-ciliary pumping region, the resistance of pressure rise over wavelength $\Delta p_\lambda > 0$ (adverse pressure) is overcome by the peristalsis-cilia, and the flow takes place in the direction of propagation of the travelling wave. The region in which flow takes place in a direction opposite to the propagation of the travelling wave because of the dominance of pressure rise over wavelength $\Delta p_\lambda > 0$ over peristalsis-cilia terms as the retrograde pumping region. In the augmented pumping region, the pressure drop over wavelength $\Delta p_\lambda < 0$ (favourable pressure) assists the flow due to the peristalsis-cilia of the tube. Figures 9(a) and 9(b) are prepared to observe the effects of the metachronal wave parameter ϵ and the amplitude ratio ϕ on the pumping capability. It can be inferred from these figures that the pumping rate increases in the retrograde and peristaltic-ciliary pumping regions as ϵ and ϕ are incremented. An opposite behavior is observed for increasing ϵ and ϕ on the pumping rate in the augmented pumping region, i.e., an increase in ϵ and ϕ causes diminishment in the pumping rate in the augmented pumping region. Comparison between the pumping characteristics of the peristaltic flow (when $\epsilon = 0.00$) and the peristaltic-ciliary flow (when $\epsilon = 0.15$) is elaborated in Fig. 9(c). This comparison enables us to reveal the fact that, the pumping rate of the peristaltic flow is smaller in the retrograde and peristaltic-ciliary pumping regions, while it is bigger in the augmented pumping region than that of the peristaltic-ciliary flow. Inclusion of swaying motions of the cilia tips along with peristaltic contractions of the tube surface causes lessening of pumping rate in the augmented pumping region.

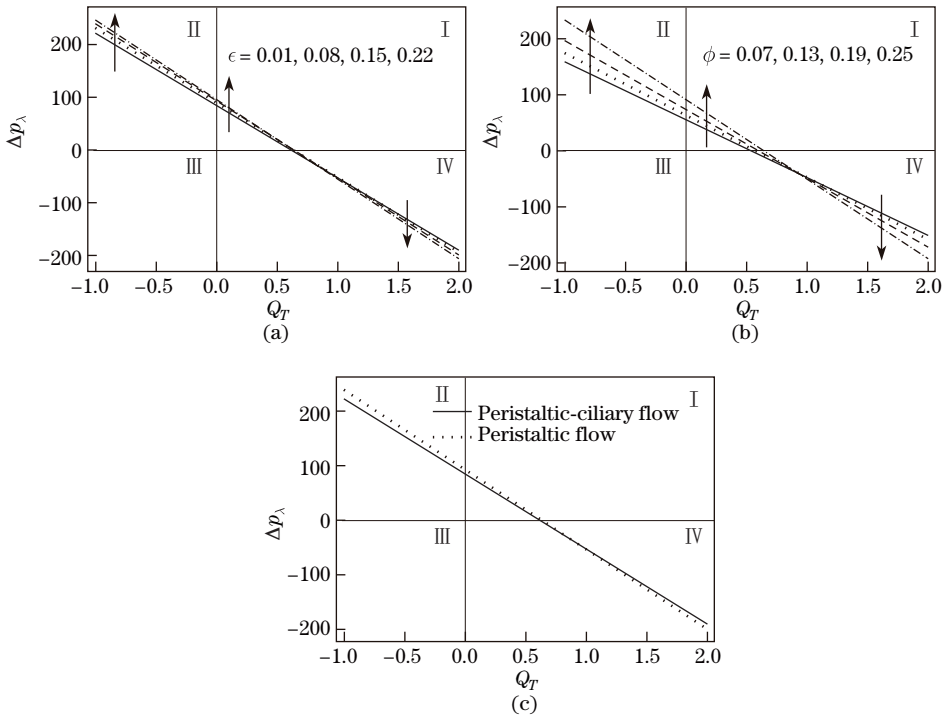

Fig. 9 Pressure difference over wavelength versus time mean volume flow rate profiles when there are various (a) metachronal wave parameter ϵ (when $\phi = 0.19$ and $\kappa = 1.5$) and (b) amplitude ratio ϕ (when $\epsilon = 0.08$ and $\kappa = 1.5$), and (c) for comparison between the peristaltic flow and the peristaltic-ciliary flow (when $\phi = 0.19$ and $k = 1.5$)

In the phenomenon of trapping, streamlines split and close to form a bolus which moves as a whole with the wave front. Trapping can be observed by plotting the streamlines in a moving

frame of reference[16–17]. Patterns of streamlines with trapped boluses are plotted in Fig. 10 to observe the effects of the pressure gradient at the tube entrance ξ, the metachronal wave parameter ϵ, and the amplitude ratio ϕ on trapped boluses. The trapped boluses of fluid are of elliptic shape as is seen through Fig. 10. The size of the trapped bolus can be described in terms of density of the streamlines. The trapped bolus appears in a region where the tube diameter has local maximum which continues to diminish as the tube diameter becomes local minimum. Figures 10(a)–10(d) are prepared to observe the effects of the pressure gradient at the tube entrance ξ on the size of trapped boluses. The size of trapped boluses is found to be reduced with the increment in ξ. The number of circulations decreases significantly as ξ is incremented. Figures 10(e)–10(l) display the effects of ϵ and ϕ on trapped boluses. It is speculated that with an increase in ϵ and ϕ, the size of the trapped boluses enhances. The number of circulation in a trapped bolus is also evidently increased with the increase in ϵ and ϕ. Moreover, one may also say that when the amplitudes of the sinusoidal wave and the metachronal wave are incremented, the trapping of the boluses of fluid enhances. In Figs. 10(m) and 10(n), a comparison between the size of the trapped boluses of the peristaltic flow and the peristaltic-ciliary flow is illustrated.

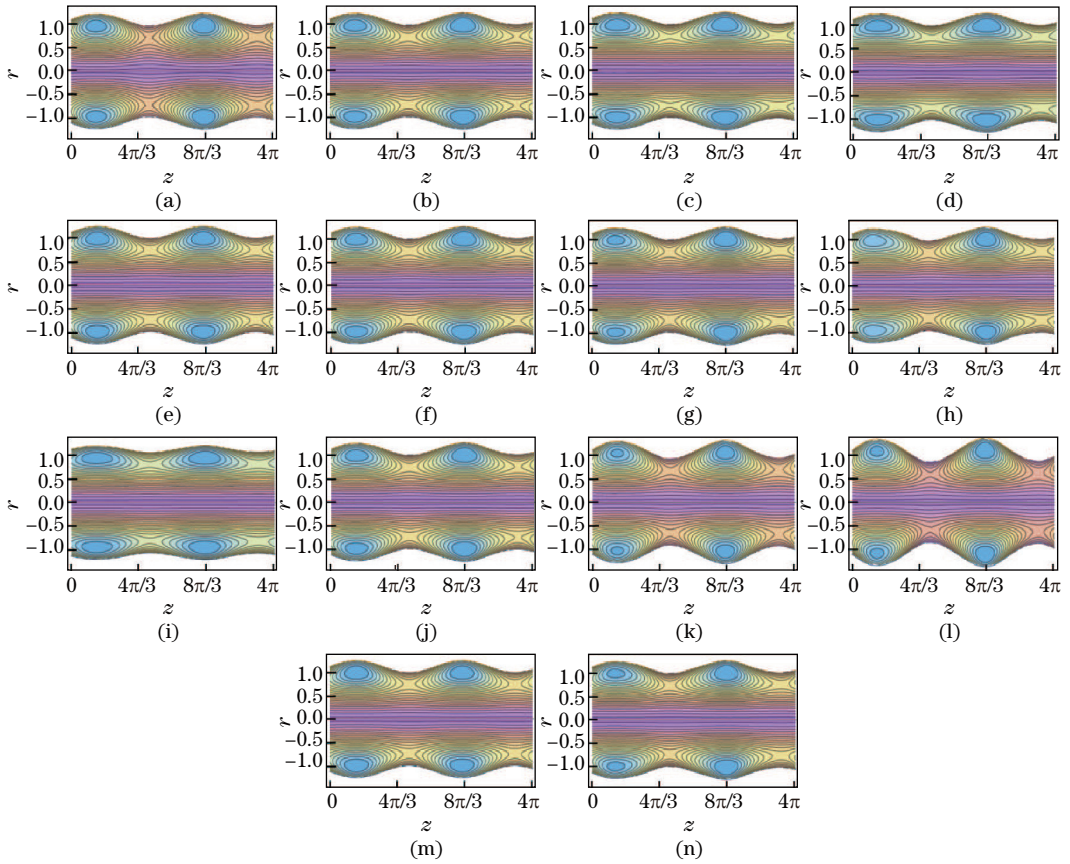

Fig. 10 Plots of streamlines with trapped boluses in a moving frame of reference when there are variations in the pressure gradient at the tube entrance ((a) $\xi = 5.0$, (b) $\xi = 7.0$, (c) $\xi = 9.0$, and (d) $\xi = 11.0$) when $\epsilon = 0.08$, $\phi = 0.13$, and $k = 1.5$, when there are variations in metachronal wave parameter ((e) $\epsilon = 0.01$, (f) $\epsilon = 0.08$, (g) $\epsilon = 0.15$, and (h) $\epsilon = 0.22$) when $\xi = 7.0$, $\phi = 0.13$, and $k = 1.5$, and when there are variations in amplitude ratio ((i) $\phi = 0.07$, (j) $\phi = 0.13$, (k) $\phi = 0.19$, and (l) $\phi = 0.25$) when $\xi = 7.0$, $\epsilon = 0.08$, and $k = 1.5$, and comparison between (m) peristaltic flow and (n) peristaltic-ciliary flow when $\xi = 7.0$, $\phi = 0.13$, and $k = 1.5$

It is delineated from this comparison that trapped boluses of the peristaltic-ciliary flow are of slightly larger size as compared with the peristaltic flow. When only peristaltic contractions of the tube surface are present, trapped boluses of smaller size are formed near the tube surface. It means that inclusion of the swaying motions of the tips of cilia along with the peristaltic contractions causes enlargement in the size of the trapped boluses.

4 Concluding remarks

In the present theoretical assessment, we model the peristalsis-cilia induced flow of linearly viscous fluid within a fallopian tubal fluid in a finite two-dimensional narrow tube. The present model theoretically assesses the peristaltic-ciliary transport of a developing embryo within the fallopian tubal fluid from the ampulla to the intramural in the human fallopian tube. The key findings of this assessment are summarized below.

(i) The axial velocity increases radially with the increase in ξ, whereas it decreases radially with the increase in ϵ and ϕ.

(ii) The axial velocity increases axially as ξ and ϕ are incremented. The increment in the value of ϵ results in the decrease of axial velocity during the first wavelength, while it results in the axial increase during the second wavelength.

(iii) The appropriate residue time over wavelength decreases with an increase in ξ, whilst it increases with an increase in ϵ and ϕ.

(iv) The volume flow rate enhances when ξ is increased, whereas it diminishes when ϵ and ϕ are increased.

(v) The pumping rate increases in the retrograde and peristaltic-ciliary pumping regions, while it decreases in the augmented pumping region with the increase in ϵ and ϕ.

(vi) The size of the trapped bolus shortens as ξ is increased. Moreover, it enlarges as ϵ and ϕ are increased.

(vii) As a special case, a comparison between the peristaltic flow and the peristaltic-ciliary flow is made.

Application of this model to assess the transport characteristics of a developing embryo within a fallopian tubal fluid in the human fallopian tube may introduce a new biomechanical factor of fertility. Increment in the appropriate residue time of the developing embryo due to the inclusion of the swaying motions of the cilia tips along with cyclic peristaltic contractions in the presence of fallopian tubal fluid, in turn helps in completing the required mitotic divisions. When the value of the pressure gradient at the entrance of ampullar region and amplitudes of both the sinusoidal and metachronal waves are controlled by some biomechanical means, one can better achieve complete, proper, and all required mitotic divisions. It is very likely that the developing embryo is transported within the fallopian tubal fluid through the fallopian tube, from the ampulla to the intramural and implanted successfully at fundus with the further aid of peristaltic contractions of the uterus surface. Otherwise, either mitotic divisions are never completed or the embryo is never able to be transported through the fallopian tube or never implanted at fundus. In such situations, an embryo with incomplete mitotic divisions leads to the abnormality or impairment in the functioning of an organ in the new born baby or an embryo is to be evacuated at the next menstruation or implanted away from fundus which ends with a miscarriage.

References

[1] Eddy, C. A. and Pauerstein, C. J. Anatomy and physiology of the fallopian tube. *Clinical Obstetrics and Gynecology*, **23**(4), 1177–1193 (1980)

[2] Yeung, W. S. B., Lee, C. K. F., and Xu, J. S. The oviduct and development of the preimplantation embryo. *Reproductive Medicine Review*, **10**(1), 21–44 (2002)

[3] Ghazal, S., Makarov, J. K., and de Jonge, C. J. Egg transport and fertilization. *Global Library of Women's Medicine*, **2014** (2014) https://doi.org/10.3843/GLOWM.10317

[4] Fauci, L. J. and Dillon, R. Biofluidmechanics of reproduction. *Annual Review of Fluid Mechanics*, **38**, 371–394 (2006)

[5] Jones, R. E. and Lopez, K. H. *Human Reproductive Biology*, Elsevier, Burlington, 253–260 (2006)

[6] Kolle, S., Reese, S., and Kummer, W. New aspects of gamete transport, fertilization, and embryonic development in the oviduct gained by means of live cell imaging. *Theriogenology*, **73**, 786–795 (2010)

[7] Sokol, E. R. Clinical anatomy of the uterus, fallopian tubes, and ovaries. *Global Library of Women's Medicine*, **2011** (2011) https://doi.org/10.3843/GLOWM.10001

[8] Carlson, B. M. *Human Embryology and Developmental Biology*, Elsevier, Philadelphia, 36–37 (2014)

[9] Ezzati, M., Djahanbakhch, O., Arian, S., and Carr, B. R. Tubal transport of gametes and embryos: a review of physiology and pathophysiology. *Journal of Assisted Reproduction and Genetics*, **31**(10), 1337–1347 (2014)

[10] Wakeley, P. W. *Optimisation and Properties of Gamete Transport*, Ph. D. dissertation, University of Birmingham, 139–166 (2008)

[11] Leese, H. J. The formation and function of oviduct fluid. *Journal of Reproduction and Fertility*, **82**, 843–856 (1988)

[12] Leese, H. J., Tay, J. I., Reischl, J., and Downing, S. J. Formation of fallopian tubal fluid: role of a neglected epithelium. *Reproduction*, **121**, 339–346 (2001)

[13] Lyons, R. A., Saridogan, E., and Djahanbakhch, O. The reproductive significance of human fallopian tube cilia. *Human Reproduction Update*, **12**(4), 363–372 (2006)

[14] Siddiqui, A. M., Farooq, A. A., and Rana, M. A. Hydromagnetic flow of Newtonian fluid due to ciliary motion in a channel. *Magnetohydrodynamics*, **50**(3), 109–122 (2014)

[15] Sadaf, H. and Nadeem, S. Influences of slip and Cu-blood nanofluid in a physiological study of cilia. *Computer Methods and Programs in Biomedicine*, **131**, 169–180 (2016)

[16] Buthaud, H. *The Influences of Unsymmetry, Wall Slope and Wall Motion on Peristaltic Pumping at Small Reynolds Number*, M. Sc. dissertation, The Johns Hopkins University Baltimore Maryland 21218, 9–24 (1971)

[17] Nadeem, S. and Shahzadi, I. Mathematical analysis for peristaltic flow of two phase nanofluid in a curved channel. *Communications in Theoretical Physics*, **64**(5), 547–554 (2015)

[18] Nadeem, S. and Shahzadi, I. Single wall carbon nanotube (SWCNT) analysis on peristaltic flow in an inclined tube with permeable walls. *International Journal of Heat and Mass Transfer*, **97**, 794–802 (2016)

[19] Nadeem, S. and Shahzadi, I. Inspiration of induced magnetic field on nano hyperbolic tangent fluid in a curved channel. *AIP Advances*, **6**(1), 015110–015125 (2016)

[20] Shahzadi, I. and Nadeem, S. Stimulation of metallic nanoparticles under the impact of radial magnetic field through eccentric cylinders: a useful application in biomedicine. *Journal of Molecular Liquids*, **225**, 365–381 (2017)

[21] Shahzadi, I., Sadaf, H., Nadeem, S., and Saleem, A. Bio-mathematical analysis for the peristaltic flow of single wall carbon nanotubes under the impact of variable viscosity and wall properties. *Computer Methods and Programs in Biomedicine*, **139**, 137–147 (2017)

[22] Shahzadi, I. and Nadeem, S. Inclined magnetic field analysis for metallic nanoparticles submerged in blood with convective boundary condition. *Journal of Molecular Liquids*, **230**, 61–73 (2017)

[23] Shahzadi, I. and Nadeem, S. Impinging of metallic nanoparticles along with the slip effects through a porous medium with MHD. *Journal of the Brazilian Society of Mechanical Sciences and Engineering*, **39**(7), 2535–2560 (2017)

[24] Shahzadi, I. and Nadeem, S. Impact of curvature on the mixed convective peristaltic flow of shear thinning fluid with nanoparticles. *Canadian Journal of Physics*, **94**(12), 1319–1330 (2016)

[25] Shahzadi, I., Nadeem, S., and Rabiei, F. Simultaneous effects of single wall carbon nanotube and effective variable viscosity for peristaltic flow through annulus having permeable walls. *Results in Physics*, **7**, 667–676 (2017)

[26] Eytan, O. and Elad, D. Analysis of intra-uterine fluid motion induced by uterine contractions. *Bulletin of Mathematical Biology*, **61**, 221–236 (1999)

[27] Eytan, O., Jaffa, A. J., and Elad, D. Peristaltic flow in a tapered channel: application to embryo transport within the uterine cavity. *Medical Engineering and Physics*, **23**, 473–482 (2001)

[28] Yaniv, S., Jaffa, A. J., Eytan, O., and Elad, D. Simulation of embryo transport in a closed uterine cavity model. *Eurpian Journal of Obstetrics and Gynecology and Reproductive Biology*, **144**(1), 50–60 (2009)

[29] Blake, J. R., Vann, P. G., and Winet, H. A model for ovum transport. *Journal of Theoretical Biology*, **102**, 145–166 (1982)

[30] Papanastasiou, T. C. *Applied Fluid Mechanics*, P T R Prentice Hall, Inc., A Paramount Communications Company Englewood Cliffs, New Jersey, 309–310 (1994)

[31] Siddiqui, A. M., Ashraf, H., Walait, A., and Haroon, T. On study of horizontal thin film flow of Sisko fluid due to surface tension gradient. *Applied Mathematics and Mechanics* (*English Edition*), **36**(7), 847–862 (2015) https://doi.org/10.1007/s10483-015-1952-9